ARTICLE

Femtosecond Two-Photon Detachment of Cu^- Studied By Photoelectron Imaging

Ben-kang Liu, Yan-qiu Wang, Li Wang*

Dalian Institute of Chemical Physics, Chinese Academy of Science, Dalian 116023, China

(Dated: Received on September 12, 2013; Accepted on October 14, 2013)

The wavelength dependence of photoelectron angular distributions (PADs) of two-photon detachment of Cu^- has been directly studied by using the photoelectron map imaging. Results show that for the laser field intensity of 6.0×10^{10} W/cm^2, PADs exhibit dramatic change with the external field wavelength. Comparison between the experimental observation and the lowest-order perturbation theory prediction indicates that the pattern of PADs can be explained by the interference of the s and d partial waves in the final state. Relative contributions of s and d partial waves in the two-photon detachment at different laser wavelengths are obtained.

Key words: Femtosecond, Two-photon detachment, Photoelectron velocity imaging, Cu^-

I. INTRODUCTION

The excess electrons in negative ions are bound in a short-range potential on the order of r^{-4} (r is the distance between the electron and the nucleus), with the H^- ion being the only exception [1]. This short-range potential gives rise to a number of exotic properties of negative ions that are different from neutral atoms or positive ions, in which electrons are bound in a long-range Coulomb potential, proportional to r^{-1}. Photodetachment of the "extra" electrons from anions has proven to be the most accurate technique for investigating the structural properties of anions. The photodetachment process is a boundary-free transition, which provides a unique opportunity to examine electron correlation effects, leaving a neutral atomic core in the presence of short-ranged potentials. Subtle interactions, such as electron correlation and relativistic effects can be investigated in photodetachment studies, which are veiled by the long-range Coulomb potential in the photoionization of neutral species or positive ions. The experimental observation of the excess-photon detachment of negative ions was reported for Cl^- and Au^- systems [2, 3] and was similar to the above-threshold ionization or excess-photon ionization in neutral or cation systems. Previous studies suggested that the detachment process near the negative threshold followed the Wigner threshold law [4, 5]. In the vicinity of the detachment threshold, the photodetachment cross section has the form

$$\sigma \propto E^{2l+1} \tag{1}$$

where l is the angular momentum of the outgoing electron and E is its excess energy. The photodetachment of anions in the vicinity of the detachment threshold has drawn great attention, since in this energy range the electron-correlation effects and interferences become more prominent.

The photoelectron velocity mapping technique provides a valuable approach for investigating the photodetachment of anions [6, 7]. The photoelectron angular distributions (PADs) carry the signature of the electronic structure of the anion, the neutral species and the symmetry of the wave function for the detached electron [8, 9], which may provide insight into the partial wave composition of the molecular orbitals through which the detachment process occurs [6, 10−12]. PADs are typically well described by the single-electron model in which the orbital angular momentum of the incoming photon is coupled only to the detaching electron neglecting all interactions involving the neutral core [13, 14]. Thus, emission from an s-orbital yields a β value of +2, while emission from a p-orbital (or higher orbital angular momentum state) results in two partial waves that can interfere to yield any β value between −1 and +2. However, near the autoionization and autodetachment resonances threshold, electron correlations could be significant and could induce a twist in the spectral dependency of the asymmetry parameters, as predicted theoretically [15] and observed experimentally near the autoionizing resonances of two-photon-excited iodine atoms [16]. Significant electron correlations in either the initial bound or final continuum state change the asymmetry parameter from that predicted by the single-electron model. Remarkable deviations in the asymmetry parameter can provide a convenient probe for autodetachment resonances. Experimental probing of such a deviation from the single-electron model is

*Author to whom correspondence should be addressed. E-mail: Liwangye@dicp.ac.cn, Tel.: +86-411-84379243

necessary in anions whose electronic structure and dynamics are largely determined by the electron correlations [17]. Recent photodetachment experiments of sodium cluster anions have indicated that PADs deviate strongly from the predictions of single-electron models, indicating that the correlated multi-electron effects play a distinct role in the photoemission process [18].

Previous studies on detachment of H^- indicated that two-photon detachment was different from one-photon process. The PAD in the two-photon detachment was found to change dramatically with laser intensity. At the lower intensity, 1.3×10^{11} W/cm^2, the PAD had a maximum distribution along the direction of the laser polarization, which could be described by a superposition of s and d waves with their relative phase taken into account. At an intensity of 6.5×10^{11} W/cm^2, the PAD had a bell-like appearance with the maximum pointing perpendicular to the laser polarization. The semiclassical Keldysh-Faisal-Reiss (KFR) theory was used to explain this behavior [19]. The detached electron could tunnel into the continuum at different times within a period of the field oscillation, resulting in a continuum of wave functions with different phases at which electrons were emitted. The superposition of these wave functions with different phases led to a specific PAD dependence on the laser intensity. Non-perturbative Floquet theory predicted that, while the laser field intensity was fixed, similar effects would be observed under different laser frequencies [20]. In multiphoton detachment by a linearly polarized laser field, the quantum interference effects of the electrons emitted in such a process show a characteristic distribution in the angle-resolved energy spectrum [19, 21]. Semi-analytical approaches, such as the adiabatic saddle-point model of Gribakin and Kuchiev [23] based on the Keldysh approximation [24], have been successfully applied in quantitatively describing the interaction of negative atomic ions with femtosecond [22, 25] and few-cycle ultrafast infrared laser fields [26]. The dependence of PADs on the laser intensity was predicted theoretically by the time-dependent Schrödinger equation using the Sturmian-Floquet approach [27].

Multi-photon ionization of atoms or molecules and multi-photon detachment of negative ions in an ultrafast laser field are very interesting non-perturbative quantum mechanical phenomena, which have been a hot topic of chemical physics in the past two decades both theoretically and experimentally [1, 19, 22−29]. Theoretically, multi-photon detachment is well described by the quantum-mechanical models based on the strong-field approximation (SFA) [24]. Negative ions represent such a structure, which constitutes simpler systems than neutral atoms due to the absence of the net Coulomb attraction between the active electron and neutral atom. The Coulomb effects are the main problem of the SFA, which fails to explain the low-energy spectra in some laser parameters regimes. In addition, the atomic potential for negative ions can be well modeled by a zero-range potential [30]. So the multi-photon detachment of negative ions has been treated as an ideal process to verify the SFA theory.

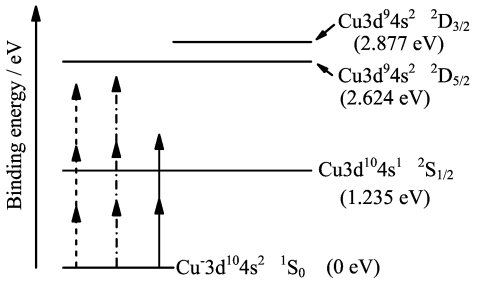

FIG. 1 Simplified energy-level diagram for Cu and Cu^-. Energies of neutral-atom states are marked with respect to the ground state of Cu^-. Three laser wavelengths of 1448 nm (solid arrow), 1495 nm (dash dot arrow), 1597 nm (dash arrow) are investigated in this work

In this work, we report on the wavelength dependence of two-photon detachment of Cu^-. Cu^- has been extensively studied with one-photon detachment for probing the electron-electron correlation effects [12, 31, 32]. An energy-level diagram of the relevant states is shown in Fig.1, based upon these previous researches [33, 34]. Our femtosecond two-photon detachment experiments of Cu^- indicate that the PADs has an unusual shape with a maximum pointing perpendicular to the laser polarization, and the relative intensities of different components in PADs change intensively with the laser wavelengths. An adiabatic-theory approach to the multiphoton problems proposed by Gribakin and Kuchiev [23] is applied for understanding our observations. Relative contributions from s and d partial waves in the two-photon detachments at different laser wavelengths are also obtained.

II. EXPERIMENTS

The experimental setup for studying photodetachment of anions is illustrated in Fig.2(a). Copper anions are formed from a laser vaporization metal cluster source in which the second harmonic output (532 nm) of a neodymium-doped yttrium aluminum garnet laser (YAG laser, Quantel Brilliant) with a pulse duration of 5 ns operating at 20 Hz is focused on a rotating and translating copper rod to form a plasma shown in Fig.2(b). The metal plasma is then cooled using a helium carrier gas (99.9%) at a stagnation pressure of 0.4 MPa and is expanded into a vacuum through a pulsed valve (General Valve Corp.). As shown in Fig.2(a), the central portion of the negative ions is extracted perpendicularly and accelerated into a McLaren-Wiley TOF mass spectrometer using a −1.4 kV high-voltage pulse.

Mass selection is achieved via three electrodes with a time-delayed, pulsed electric field applied to the cen-

DOI:10.1063/1674-0068/27/02/125-130

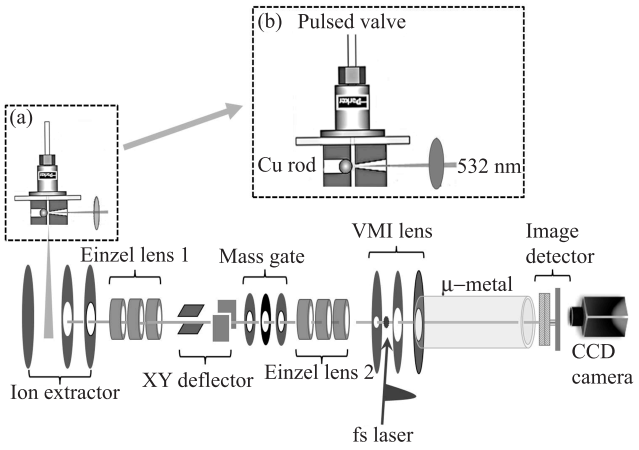

FIG. 2 Schematic drawing of the experimental setup. (a) Laser vaporization metal cluster source, (b) details of laser vaporization metal cluster source.

tral electrode. The selected negative ions are then refocused onto the center of a time-delayed, pulsed velocity-mapping two-stage electric field and are photodetached by a time-delayed femtosecond laser pulse. The detached photoelectrons are accelerated and velocity-focused toward a position-sensitive detector. After flying through a 40 cm field-free region, which is shielded against stray magnetic fields by a μ-metal tube, the photoelectrons are mapped onto a two-stage microchannel plate (MCP) detector backed by a phosphor screen. Images on the screen are captured using a thermoelectrically cooled charge-coupled device video camera (LAVISION Inc. Imager QE). All photoelectron images are reconstructed using the pBASEX program [35, 36], which can yield both the photoelectron energy spectra and the PADs [37].

Linearly polarized laser wavelengths of 1448, 1495, and 1597 nm are generated in a commercial optical parametric amplifier (Quantronix/Light Conversion, TOPAS) pumped by the fundamental output (centered at 817 nm with a 30 nm FWHM bandwidth and a 70 fs pulse width) of a solid-state femtosecond laser at a 20 Hz repetition rate with a 10 mJ/pulse. The laser pulse width is determined via single-shot intensity autocorrelation. The pulse energies at these wavelengths are maintained at approximately 200 μJ in the interaction region. The laser beam is focused with a 50 cm focal-length lens with a polarization direction parallel to the detector plane.

III. RESULTS AND DISCUSSION

Figure 3 illustrates the femtosecond photodetachment results of Cu^- at 1448, 1495, and 1597 nm at a fixed intensity of 6.0×10^{10} W/cm^2. The kinetic energy of detached photoelectron can be described as

$$E_k = 2E_v - E_{\rm d} \qquad (2)$$

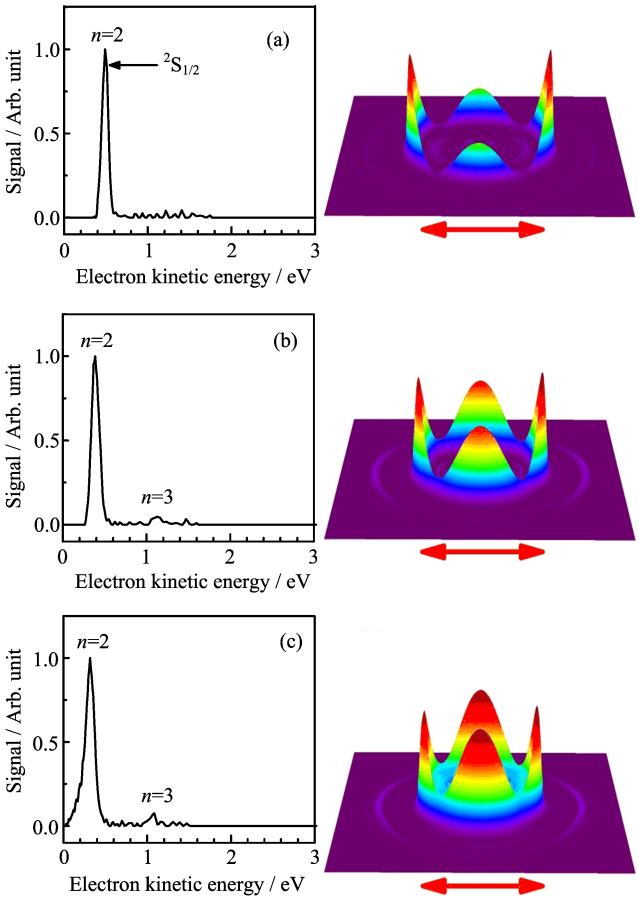

FIG. 3 Photodetachment results of Cu^- at (a) 1448 nm, (b) 1495 nm, and (c) 1597 nm at a fixed intensity of 6.0×10^{10} W/cm^2. Right column: reconstructed photoelectron images, left column: the corresponding photoelectron spectra. Double arrow lines in right column represent the directions of the laser polarization.

where E_v is the one photon energy, and $E_{\rm d}$ is the electron detachment energies, 1.235 eV for Cu^- [33, 34]. The largest peaks in the photoelectron kinetic energy spectra (PES) in Fig.3 represent the two-photon detachment channels of Cu^- ($^1S_0+2h\nu\rightarrow{}^2S_{1/2}+e^-$). Weak peaks in PES, correspond to the first-order above threshold detachment, three-photon detachment, ($^1S_0+3h\nu\rightarrow{}^2S_{1/2}+e^-$) of Cu^-. Currently, we mainly focus on the two-photon detachment process of Cu^-. The laser intensities at these wavelengths are carefully controlled to maximize the two-photon detachment signals and to minimize the unexpected multiphoton detachment processes, such as three- or four- photon process. The laser peak intensities in the interaction region are estimated to be about 6×10^{10} W/cm^2 at these wavelengths by measuring the focus size based on the pinhole method. As shown in Fig.3, one can visually conclude that the angular distributions of photoelectron from the two-photon detachments change dramatically with the laser wavelengths.

DOI:10.1063/1674-0068/27/02/125-130

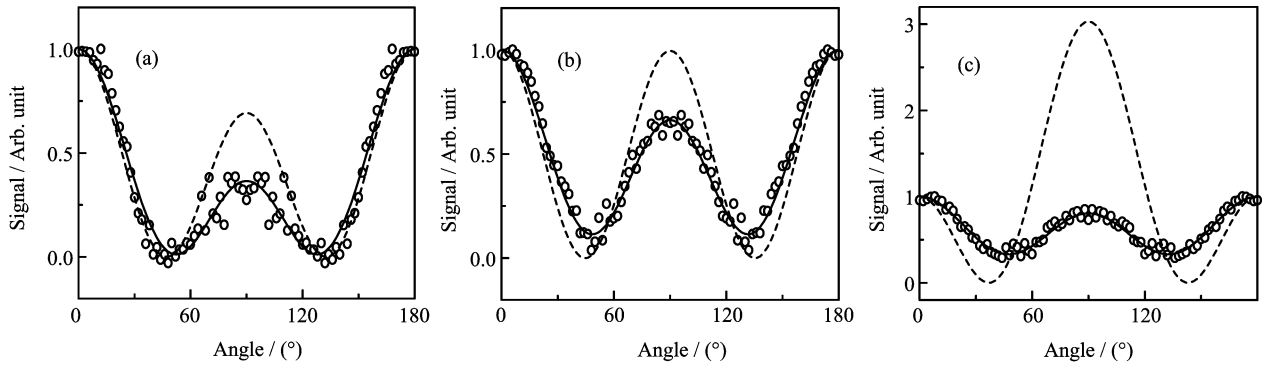

FIG. 4 PADs of the two-photon detachment of Cu^- at (a) 1448 nm, (b) 1495 nm, and (c) 1597 nm at a fixed intensity of 6.0×10^{10} W/cm^2. Circle symbol: the experimental data; solid lines: the fitting results, dashed lines: the theoretical calculations.

Figure 4 illustrates the PADs of the two-photon detachment channel of Cu^- at given laser intensities and these three wavelengths. Clearly, the PADs consist of main lobes (along the directions of the laser polarization) and central jets (perpendicular to the laser polarization). Relative intensities of the central jet to that of the main lobe vary with the laser wavelength, as shown in Fig.4. The pattern of the PADs of two-photon detachment of Cu^- is similar to that found in the experiment on two-photon detachment of H^- and X^- (X=F, Br) for they represent a negative ion with a short-range interaction between the loosely bound electron and the core [19, 22]. In the case of X^- (X=F, Br) [22], since the laser intensity in the detachment experiment was about 6.0×10^{14} W/cm^2, the angle resolved momentum distribution consisted of a few excess photon detachment peaks, which were due to ponderomotively broadening effect. At higher electron momenta, however, there were the well-pronounced jets pointing along the laser polarization direction, which were supposed to be due to the contribution from the subsequent ionization of neutral atom (the sequential double detachment) [22]. In our experiments, the laser intensity is kept at about 6.0×10^{10} W/cm^2, which is much lower than the experimental laser conditions in Refs.[19, 22]. The sequential double detachment process cannot be reachable and the ponderomotive energy shift is estimated less than 0.01 eV.

As illustrated in Fig.3, it is evident that the ratio of the height of the central jets to that of the main lobes increases with the laser wavelength. Similar to the wavelength dependence, this PAD behavior can be attributed to the Wigner threshold law [5]. As explained by Telnov and Chu [20], when the laser intensity increases with a fixed wavelength, the larger ponderomotive shift results in a drift of the two-photon detachment channel towards the detachment threshold, which changes the relative contributions of the s and d waves to the detachment amplitude and, as a result, the shape of the PADs.

The PAD patterns of two-photon detachment of Cu^- are similar to those fine structures in the two-photon detachment experiments of H^- and X^-[19, 22]. An adiabatic-theory approach to the multiphoton problems proposed by Gribakin and Kuchiev were successfully applied in describing multiphoton detachment results of H^- and X^- [23]. In this theory, a saddle-point method have been used to give a simple analytical solution to the problem of multi-photon detachment by a monochromatic linearly polarized laser field $\mathbf{F}(t)=\mathbf{F}\cos\omega t$. The differential n-photon detachment rate of negative ion for the electron in the initial state l, m can be represented as Eq.(3):

$$\frac{\mathrm{d}\omega_n}{\mathrm{d}\Omega}=\frac{pA^2}{4\pi}(2l+1)\frac{(l-|m|)!}{(l+|m|)!}\left|P_l^{|m|}\cdot\sqrt{1+p^2\sin^2\frac{\theta}{\kappa^2}}\right|^2\left|\sum_{\mu=1,2}(\pm)^{l+m}\frac{(c_\mu+is_\mu)^n}{\sqrt{2\pi(-iS''_\mu)}}\cdot\exp[-ic_\mu(\xi+zs_\mu)]\right|^2 \tag{3}$$

$$p=\sqrt{2\left(n\omega-\frac{F^2}{4\omega^2}+E_0\right)} \tag{4}$$

$$z=\frac{F^2}{4\omega^3} \tag{5}$$

$$\xi=\frac{Fp\cos\theta}{\omega^2} \tag{6}$$

$$s_\mu=\frac{-\xi\pm i\sqrt{8z(n-z)-\xi^2}}{4z} \tag{7}$$

$$c_\mu=\pm i\sqrt{1-s_\mu^2} \tag{8}$$

$$S''_\mu=c_\mu(\xi+4zs_\mu) \tag{9}$$

where ω_n is the total n-photon detachment rate, $\mathrm{d}\omega_n/\mathrm{d}\Omega$ is the differential n-photon detachment rate, A=1.2 is the asymptotic parameter of the bound-state radial wavefunction of the ground state of Cu^-, p is the photoelectron momentum, θ is the emission angle

DOI:10.1063/1674-0068/27/02/125-130

with respect to the polarization axis, $P_l^{|m|}$ is the associated Legendre function, κ is determined by the energy of the bound state $E_0=-\kappa^2/2$, F is the field strength of the laser field, ω is the frequency of the laser field, n is the number of the photons. The signs $\pm$ in the s_μ and c_μ correspond to the two saddle points μ=1,2. An explicit expression for the saddle points can be found in Ref.[23].

As illustrated in Fig.4, the oscillatory features at different laser wavelengths are reproduced well. According to the theory, these oscillatory behaviors can be attributed to the quantum interference from the two saddle point contributions. Although the main characters are quite close to the experimental results, the magnitudes between theoretical calculations and experimental results differ significantly at particular angles. This disagreement may be due to several reasons. The important features of ultrafast laser, the carrier envelope phase and the cycle number, may play a crucial role in the nonlinear interaction with matter [20, 28, 38], and current theory does not consider these parameters. In addition, Keldysh-based theories are based upon one-electron approximation, while many-electron effects are well known to affect significantly both the electron structure and the photodetachment of negative ions. Furthermore, the dipole moment, induced by the outer electron in the atomic core due to the ac field [39], may also be a key factor, which is not considered in these theoretical approaches. Evidently, accurate theoretical approach is needed for fully understanding the two-detachment of anions by femtosecond laser.

The dramatic changes in PADs with the laser wavelength can be understood as the Wigner threshold effect [5]. Based upon the Wigner threshold law, the lowest-order perturbation theory (LOPT) were proposed for understanding the two-photon detachment process by intense laser field [20]. It has been proven that even for the intensity as high as 6.5×10^{11} W/cm^2, PADs can be well described by LOPT in the two-photon detachment amplitude [20]. Thus, we can expand the PADs as a function of the angle θ between the detection and laser field directions on the basis of the Legendre polynomials.

$$\frac{\mathrm{d}\Gamma_n}{\mathrm{d}\Omega} = \frac{\Gamma_n}{4\pi}\left[1+\sum_{l=1}^{\infty}\beta_{2l}^{(n)}P_{2l}(\cos\theta)\right] \tag{10}$$

where $\beta_{2l}^{(n)}$ are the anisotropy parameters, and $P_{2l}(x)$ is the Legendre polynomials. For the two-photon detachment, according to LOPT, the emitted electrons in this case may possess the angular momentum 0 or 2, then, the detachment amplitude should behave as follows:

$$A_n = \delta\sqrt{1/2}P_0(\cos\theta) + \sqrt{5/2}P_2(\cos\theta) \tag{11}$$

where A_n is the photodetachment amplitude, factors $\sqrt{1/2}$ and $\sqrt{5/2}$ are added as normalization coefficients for the Legendre polynomials. The mixing coefficient δ can be calculated by fitting the PADs:

$$\mathrm{Re}\delta = \frac{9\beta_2/\beta_4 - 5}{7\sqrt{5}} \tag{12}$$

$$|\delta| = \sqrt{18/7\beta_4 - 1} \tag{13}$$

Contributions of s and d partial waves can be expressed as follows

$$P_\mathrm{s} = \frac{|\delta|^2}{1+|\delta|^2} \tag{14}$$

$$P_\mathrm{d} = \frac{1}{1+|\delta|^2} \tag{15}$$

Therefore, contributions of s and d partial waves can be obtained by fitting the experimental results using Eqs.(11)−(16), as illustrated in Fig.4. The wavelength dependent partial-wave amplitudes with the fitting results of experimental PADs are list in Table I. The two saddle-point approach [23], which is the basis of our data analysis, is developed for describing the quantum interference between the two detachment points in each optical cycle. Therefore, contributions from different partial waves determine the final PAD pattern. As indicated in Table I, the relative contributions of s and d partial waves change heavily with the laser wavelength. According to the adiabatic-theory [23], different contributions from the two quantum detached channels result in the final changing PADs. Therefore, the relative contributions of s and d partial waves in Table I, obtained from the experimental varying PADs reflect the interference effects at different laser wavelengths. The s wave dominates in the vicinity of the threshold. The tendency is indeed consistent with the Wigner threshold law.

TABLE I Anisotropy parameters and partial-wave contributions of the two-photon detachment channel.

Wavelength/nm	β_2	β_4	P_s	P_d
1448	0.76±0.05	2.40±0.08	4%	96%
1495	−0.11±0.02	1.62±0.02	37%	63%
1597	−0.15±0.02	0.92±0.02	64%	36%

IV. CONCLUSION

In summary, we have presented the wavelength dependence of PADs after two-photon detachment of Cu^- which employs a photoelectron velocity map imaging. The quantum interference effect is observed in the PADs of the experiment. Our analysis shows that for the laser field at different wavelength, the shape of PADs exhibit interference of s and d partial wave in the final state of the photoelectron. For the longer wavelength, the shape of PADs changes in accordance with the Wigner threshold law when the two-photon threshold is approached,

DOI:10.1063/1674-0068/27/02/125-130

manifesting the increase of the relative weight of the s electrons. The KFR theory of Gribakin and Kuchiev is also used to simulate our experiment. However, the agreement between the experimental and theoretical results is far from satisfication. Further theoretical investigations of the strong-field interaction of negative copper ions are required.

V. ACKNOWLEDGMENTS

This work was supported by the National Natural Science Foundation of China (No.21073188).

[1] T. Andersen, Phys. Rep. **394**, 157 (2004).
[2] M. D. Davidson, H. G. Muller, and H. B. van Linden van den Heuvell, Phys. Rev. Lett. **67**, 1712 (1991).
[3] H. Stapelfeldt, P. Balling, C. Brink, and H. K. Haugen, Phys. Rev. Lett. **67**, 1731 (1991).
[4] R. Trainham, G. D. Fletcher, and D. J. Larson, J. Phys. B **20**, L777 (1987).
[5] E. P. Wigner, Phys. Rev. **73**, 1002 (1948).
[6] J. J. Melko and A. W. Jr. Castleman, Phys. Chem. Chem. Phys. **15**, 3173 (2013).
[7] R. Mabbs, E. Surber, L. Velarde, and A. Sanov, J. Chem. Phys. **120**, 5148 (2004).
[8] K. J. Reed, A. H. Zimmerman, H. C. Andersen, and J. I. Brauman, J. Chem. Phys. **64**, 1368 (1976).
[9] M. S. Bowen and R. E. Continetti, J. Phys. Chem. A **108**, 7827 (2004).
[10] E. Surber, R. Mabbs, T. Habteyes, and A. Sanov, J. Phys. Chem. A **109**, 4452 (2005).
[11] S. M. Bellm and K. L. Reid, Chem. Phys. Lett. **395**, 253 (2004).
[12] M. A. Sobhy and A. W. Jr. Castleman, J. Chem. Phys. **126**, 154314 (2007).
[13] G. Aravind, A. K. Gupta, M. Krishnamurthy, and E. Krishnakumar, Phys. Rev. A **76**, 042714 (2007).
[14] J. Cooper and R. N. Zare, J. Chem. Phys. **48**, 942 (1968).
[15] A. N. Grum-Grzhimailo, S. Fritzsche, P. O'Keeffe, and M. Meyer, J. Phys. B **38**, 2545 (2005).
[16] S. Tauro and K. P. Liu, J. Phys. B **41**, 225001 (2008).
[17] G. Aravind, N. Bhargava Ram, A. K. Gupta, and E. Krishnakumar, Phys. Rev. A **79**, 043411 (2009).
[18] C. Bartels, C. Hock, J. Huwer, R. Kuhnen, J. Schwöbel, and B. von Issendorff, Science **323**, 1323 (2009).
[19] R. Reichle, H. Helm, and I. Y. Kiyan, Phys. Rev. Lett. **83**, 243001 (2001).
[20] D. A. Telnov and S. I. Chu, Phys. Rev. A **66**, 063409 (2002).
[21] B. Bergues and I. Y. Kiyan, Phys. Rev. Lett. **100**, 143004 (2008).
[22] J. Pedregosa-Gutierrez, P. A. Orr, J. B. Greenwood, A. Murphy, J. T. Costello, K. Zrost, T. Ergler, R. Moshammer, and J. Ullrich, Phys. Rev. Lett. **93**, 223001 (2004).
[23] G. F. Gribakin and M. Y. Kuchiev, Phys. Rev. A **55**, 3760 (1997).
[24] L. V. Keldysh, Zh. Eksp. Teor. Fiz. **47**, 1945 (1964).
[25] B. Bergues, Y. F. Ni, H. Helm, and I. Y. Kiyan, Phys. Rev. Lett. **95**, 263002 (2005).
[26] S. F. C. Shearer and C. R. J. Addis, Phys. Rev. A **85**, 063409 (2012).
[27] K. Krajewska, I. I. Fabrikant, and A. F. Starace, Phys. Rev. A **74**, 053407 (2006).
[28] J. Yu, C. C. Shu, W. H. Hu, and S. L. Cong, J. Theor. Comput. Chem. **9**, 785 (2010).
[29] Y. Z. Liu, C. C. Qin, S. Zhang, Y. M. Wang, and B. Zhang, Acta Phys. Chim. Sin. **27**, 965 (2011).
[30] N. L. Manakov and A. G. Fainshtein, Zh. Eksp. Teor. Fiz. **79**, 751 (1980).
[31] A. M. Covington, S. S. Duvvuri, E. D. Emmons, R. G. Kraus, W. W. Williams, J. S. Thompson, D. Calabrese, D. L. Carpenter, R. D. Collier, T. J. Kvale, and V. T. Davis, Phys. Rev. A **75**, 022711 (2007).
[32] G. Aravind, N. B. Ram, A. K. Gupta, and E. Krishnakumar, Phys. Rev. A **79**, 043411 (2009).
[33] J. Ho, K. M. Ervin, and W. C. Lineberger, J. Chem. Phys. **93**, 6987 (1990).
[34] J. Sugar and A. Musgrove, J. Phys. Chem. Ref. Data **19**, 527 (1990).
[35] A. T. J. B. Eppink and D. H. Parker, Rev. Sci. Instrum. **68**, 3477 (1997).
[36] P. O'Keeffe, P. Bolognesi, M. Coreno, A. Moise, R. Richter, G. Cautero, L. Stebel, R. Sergo, L. Pravica, Y. Ovcharenko, and L. A. Avaldi, Rev. Sci. Instrum. **82**, 033109 (2011).
[37] B. K. Liu, Y. Q. Wang, and L. Wang, J. Phys. Chem. A **116**, 111 (2012).
[38] D. B. Milošević, G. G. Paulus, D. Bauer, and W. Becker, J. Phys. B **39**, R203 (2006).
[39] V. E. Chernov, I. Yu. Kiyan, H. Helm, and B. A. Zon, Phys. Rev. A **71**, 033410 (2005).

DOI:10.1063/1674-0068/27/02/125-130